CHINESE OPTICS LETTERS

Vol. 21, No. 11 | November 2023

Improvement of Raman spectrum uniformity of SERS substrate based on flat electrode

Zhihui Jiang (江志辉)[1], Shen Zhang (张 申)[1], Congxi Song (宋从喜)[1], Hongmin Mao (毛红敏)[1], Xin Zhao (赵 鑫)[2], Huanjun Lu (陆焕钧)[1*], and Zhaoliang Cao (曹召良)[1**]

[1] Jiangsu Key Laboratory of Micro and Nano Heat Fluid Flow Technology and Energy Application, School of Physical Science and Technology, Suzhou University of Science and Technology, Suzhou 215009, China

[2] School of Chemistry and Life Sciences, Suzhou University of Science and Technology, Suzhou 215009, China

*Corresponding author: luhuanjun@usts.edu.cn

**Corresponding author: caozl@usts.edu.cn

Received January 6, 2023 | Accepted July 6, 2023 | Posted Online November 1, 2023

The distribution of metal nanoparticles on the surface of a surface enhancement Raman scattering (SERS)-active substrate plays a prominent part in not only the enhancement of Raman vibration signal, but also the spectrum uniformity. Here, a facile method to fabricate SERS substrates with excellent homogeneity and low cost was proposed, in which a lyotropic liquid crystal soft template was introduced for the coordinated growth of the silver nanoflowers in the process of electrochemistry deposition. Simulation was carried out to illustrate the dominated influence of the distance of electrodes on the deposited nanoparticle number. Two kinds of conductive materials, silver plate and indium tin oxide (ITO) glass, were chosen as the anode, while the cathode was fixed as ITO glass. The simulated conjecture on the effect of electrode flatness on the uniformity of deposited nanoparticles in silver is experimentally proved. More importantly, it was demonstrated that with a relatively smooth and flat ITO glass anode, a SERS substrate featuring higher spectrum uniformity could be achieved. This work is of great significance to the actual applications of the SERS substrate for quantitative detection with high sensitivity.

Keywords: SERS; Raman spectrum; surface flatness; nanoparticle distribution; electrodeposition.
DOI: 10.3788/COL202321.113001

1. Introduction

Raman spectroscopy is widely used in various biochemical fields such as food safety, pharmaceutical manufacturing, and environmental protection, due to its capabilities in molecular structure identification and biological detection[1-5]. To improve the analysis sensitivity, the surface enhancement Raman scattering (SERS) technique was discovered and developed[6-9], which realized the trace or even single molecule detection of the material[10,11]. The prominent performance of SERS mainly benefits from the significant electromagnetic focusing field enhancements brought by "hot spots" generated from the nanostructures on the SERS substrates[12-17]. In the past decades, enormous attentions have been focused on the fabrication of low cost, uniform, reproducible, and efficient SERS substrates[18-23].

SERS signal inhomogeneity is a significant and long-lasting issue, resulting from inconsistent electromagnetic field distribution caused by nonuniform SERS substrates[24-29]. This restricts the actual applications of the SERS substrate for the quantitative detection and analysis of the material. Currently, the reproducibility and homogeneity of SERS substrates are normally accomplished by advanced lithographic techniques[30-32], producing highly regular and periodic surface nanostructures, including gaps, tips, holes, ridges, triangular nanoprisms and nanocones, and so on[33-39]. However, the substrate is expensive, and the fabrication process is complicated, which would not be acceptable in commercial applications.

To solve this problem, in 2017, a lyotropic liquid crystal (LC) soft template method was proposed by our group, and a well-distributed flower-like silver nanostructures substrate was successfully prepared with high sensitivity[40,41]. In 2019, Li *et al.* fabricated low-cost and recyclable 3D shell-core nanostructures through a chemical reduction reaction[42]. These low-cost and simple preparation methods further promote the commercial applications of the SERS substrate. However, compared with the substrate fabricated with lithography, the spectrum uniformity of the SERS substrate is weaker while it is prepared with these low-cost methods. For improving the spectrum uniformity of the SERS substrate, our work group proposed a surface coverage method, in which the relation between the duty cycle of the nanostructure and the spectrum intensity was obtained and

the spectrum uniformity was improved with the data processed[43,44]. However, as this method is complicated and it depends on the computation, it is unsuitable for actual applications of the SERS substrate.

In this work, based on the lyotropic LC soft template method, a direct and simple method was proposed to improve the spectrum uniformity of the SERS substrate. Concretely, the flat electrode method was demonstrated, and the effect of the electrode surface flatness was systematically investigated. Further, two types of electrodes, silver plate and indium tin oxide (ITO) glass, were chosen and compared. Consequently, the spectrum uniformity of the SERS substrate was improved greatly with the flat electrode. The results show that the SERS substrate is feasible for use as a commercial product for trace detection of the material.

2. Simulation

The SERS substrate is prepared by using a lyotropic LC soft template with the traditional electrochemical deposition method, as shown in Fig. 1. At first, an LC cell is fabricated with two electrode plates. Then, it is placed into the lyotropic LC, and the voltage is applied to prepare the SERS substrate. The electrode surface is normally rough and uneven, rather than ideally smooth. When the metal ions are electrodeposited, the unflatness of the electrodes will make the anode and cathode have different distances at different positions, which may also result in varied electrical force and deposition speed, and ultimately affect the number of metal particles deposited on the cathode surface. In this case, even under the same reaction condition, the number of metal particles deposited on the electrode surface may change with position as well. Hence, the flatness of the two electrode plates will affect the distribution of silver nanoparticles and the Raman spectrum uniformity of the SERS substrate. The simulation was performed according to the following equation:

$$N = N_1 \frac{qU}{2md} t^2, \tag{1}$$

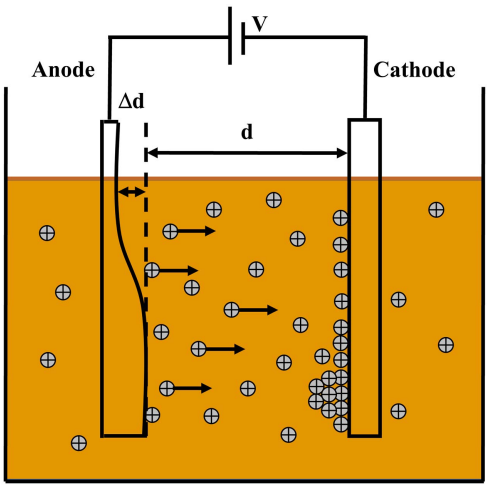

Fig. 1. Schematic diagram showing the electrodeposition process.

Table 1. Parameters Used in the Simulation.

Parameter	Definition	Value
q	Charge amount of the silver ion	1.6×10^{-19} C
U	Electrodeposition voltage	5 V
m	Mass of the silver ion	2.8×10^{-22} g
t	Electrochemical reaction time	10,800 s
N_1	Number of silver ions per unit volume	3.6×10^{7}

where q and m are the charge amount and mass of the silver ion, U and d are the voltage and spacing applied to the two electrodes, respectively, and t is the metal electrodeposition time. In the simulation, only changing the fluctuation of the anode surface changed the distance between the two electrode plates, where Δd was defined as the absolute value of the anode plate fluctuation, while the thickness of the plastic spacer was named as d (d equals 600 μm). That is, when bumps and dents appear on the surface of electrodes, the distance between the two electrodes is $d \pm \Delta d$. The necessary values of the electrochemical deposition parameters were determined based on the experimental settings and are listed in Table 1.

By changing the range of distance between the two electrodes, the relationship between the number of deposited particles and the electrode distance was simulated, as shown in Fig. 2.

It can be illustrated that the deposited particle number reduced with the increasing distance. For example, when the distance between the two electrodes changes 50 μm, the number of metal particles will vary 7.7%. It speculated that the surface flatness of the electrode plate can significantly affect the growth uniformity and spectrum consistency of the SERS substrate.

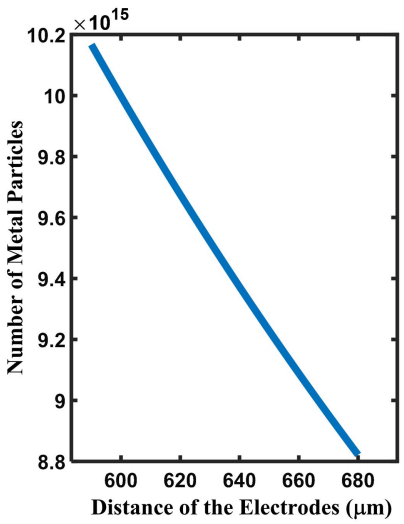

Fig. 2. Relationship between the number of deposited particles and the distance of the electrodes.

3. Experiment

3.1. Measurement of the surface flatness of the electrodes

Normally, the silver plate and ITO glass are used as the anode and cathode, respectively, to prepare the SERS substrate[40,41,43,44]. However, the silver plate is rough. So, an ITO glass is utilized to replace the silver plate as the anode. To do the comparison, the SERS substrates are fabricated, respectively, with the anodes of silver plate and ITO glass. First, the surface flatness of the silver plate and the ITO glass was scanned separately by a probe-type surface contouring instrument (DektakXT, Bruker). The selected scanning position is shown in Fig. 3. The green arrows indicate the scan direction.

The scan area was chosen as 20 mm × 15 mm (the red rectangle in Fig. 3). The scan range was set to 1 mm, and the scan time was 50 s. The measurement can obtain the surface distribution of the silver plate and the ITO glass, as well as the difference between the surface peak and valley value (PV value), which gives a quantitative comparison of the surface flatness of the two plates. According to the probe contouring measurement, the profiles showing the surface fluctuation of the two electrodes were constructed, as shown in Fig. 4.

It is apparent from the profiles that the surface of the silver plate is full of dents, while that of the ITO glass is almost smooth and only slightly bumpy in the center. Quantitatively, the PV values are 73.6 μm for the silver plate and 4.7 μm for the ITO glass. Moreover, considering that ITO glass is consumable, two more samples were tested in order to avoid the contingency, which give similar PV values of 4.6 μm and 5.2 μm. The distinct contrast of the degree of the surface fluctuation between the silver plate and the ITO glass could provide a possible reason for the remarkable difference in surface homogeneity of the SERS substrate they produced.

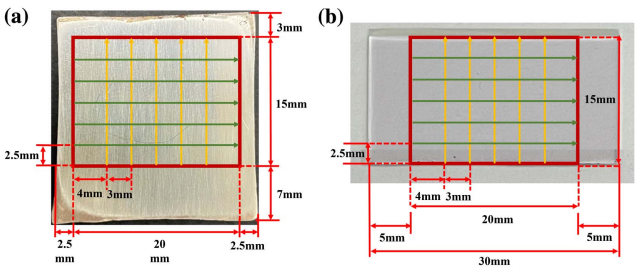

Fig. 3. Selected scan position and area of (a) the silver plate and (b) the ITO glass by the probe-type surface contouring instrument.

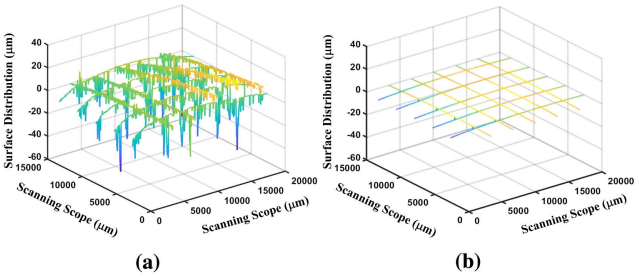

Fig. 4. Profiles of the electrode surfaces: (a) silver plate; (b) ITO glass.

3.2. Preparation and characterization of the SERS substrate

When preparing the SERS substrate with flower-like silver nanostructures, lyotropic LC was used as a soft template. The growth of the metal nanoparticles was localized in the LC cavities, which eventually accumulates on the cathode surface by electrochemical deposition. The lyotropic LC was prepared with the composition of surfactant, oil phase, and aqueous phase. In the experiment, anionic surfactant sodium bis(2-ethylhexyl) sulfosuccinate (AOT; 98%, mass fraction) was used as the surfactant; *p*-xylene (99%, mass fraction) was used as the oil phase; and the aqueous phase was designed as $AgNO_3$ solution with a concentration of 0.3 mol/L. First, 6.353 g of AOT was dissolved in 10 mL *p*-xylene and stirred until completely dissolved. Then, 2.521 mL silver nitrate solution was added dropwise with a pipette gun. The mixture was stirred for 1 h. The stirred solution was then placed in a 20°C constant temperature tank for 2 h. Microphase separation took place between the incompatible moieties, which was finally stabilized by AOT and produced a lyotropic liquid crystalline phase with a water-in-oil anti-micelle hexagonal structure, as shown in Fig. 5(a).

In order to compare the influence of the electrode surface flatness on the uniformity of the deposited nanoparticle distribution, silver plate and ITO glass were chosen as the anode, while the cathode is ITO glass. The silver plate was ground by sandpaper to remove the surface oxides. A plastic spacer with a thickness of 600 μm was used as a spacer between the electrodes. It can help keep a constant distance between the two plates. During the electrochemical deposition, the cell was

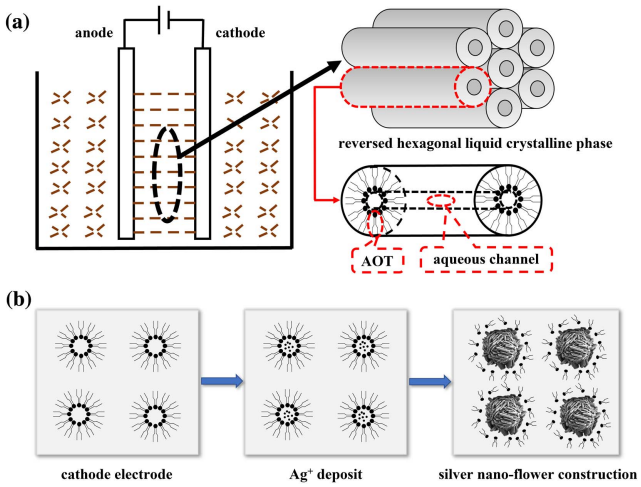

Fig. 5. Schematic representation of the electrochemical deposition of the SERS substrate: (a) phase states of lyotropic LC; (b) synergistic growth process of silver nanoflowers in electrodeposition.

immersed in the lyotropic LC. DC voltage of 5 V was applied to the two electrodes. Afterwards, the whole reaction device was placed in the 20°C constant temperature tank for 3 h.

During electrodeposition, the localized silver ions in the aqueous phase would start ordered growth within the lyotropic LC soft template. After 3 h, the silver ions nucleated gradually, which eventually broke the restriction of the soft template and deposited on the cathode surface, as shown in Fig. 5(b). After electrodeposition, the LC cartridge was immersed in analytical-reagent ethanol until the two electrode plates were separated. Cathodes covered with the nanoparticles were ultrasound cleaned using ethanol for 15 min and then dried by slow flow with N_2, which finally produced the target SERS substrate.

The surface morphology of the SERS substrate prepared with the silver plate and ITO glass as anodes was characterized by a thermal field emission scanning electron microscope (SEM, Zeiss, Baden-Wurttemberg, Germany), respectively. The extra high tension was set to 2 kV. The working distance was set to 4.1 mm.

For the SERS substrates obtained from a silver plate or ITO glass anode, SEM observations were carried out at five different positions [Fig. 6(a)]. The surface morphologies at four corners and in the middle of the substrate were recorded and compared. When the silver plate was used as the anode, obvious nonuniformity in both nanoparticle size and density was detected for the substrate [Fig. 6(b)–6(f)], although a charming nanoflower structure was formed during silver deposition [Fig. 6(g)]. It can be clearly seen that relatively smaller nanoparticles with denser packing took place at Position 5 instead of the other positions.

The same investigation was performed on the substrate from an ITO glass anode. As shown in Fig. 7, an excellent consistency was achieved. At all the five positions, the silver nanoflowers present similar size. Meanwhile, they were closely packed and almost merged to form a uniform surface.

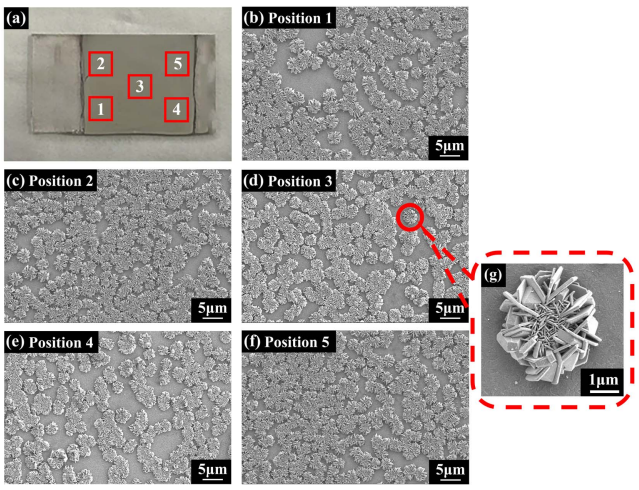

Fig. 6. SEM characterization of the SERS substrate prepared with the silver plate as an anode: (a) the five chosen positions on the fabricated SERS substrate; (b)–(f) surface morphologies at Positions 1–5; (g) zoom-in image of the formed silver nanoflower.

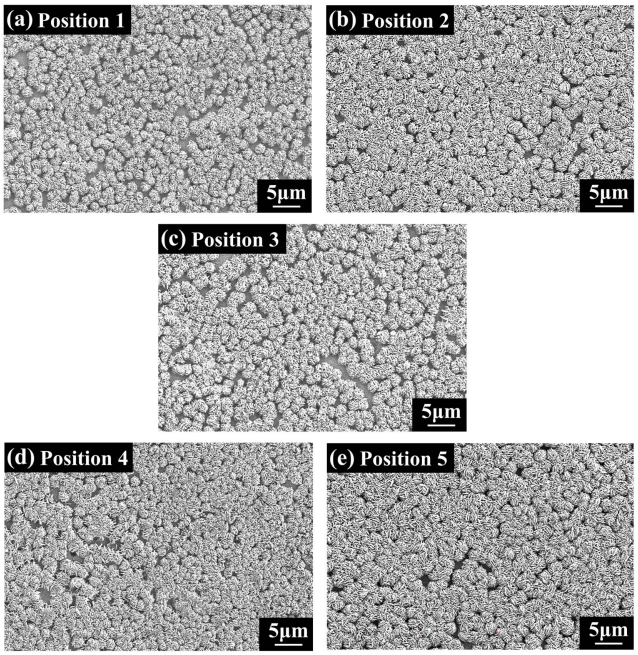

Fig. 7. (a)–(e) Surface morphologies at Positions 1–5 of the SERS substrate prepared with the ITO glass as an anode.

3.3. Calculation of the surface homogeneity of the SERS substrate

Based on the SEM results of the prepared SERS substrates, the surface coverage at different positions was calculated by image processing. The images were binarized, as shown in Fig. 8: the white area of the picture indicates the silver nanoflowers, while the black area corresponds to the gap between the nanoparticles.

To simplify the calculation, the SERS substrate is regarded as a two-dimensional plane structure. Thus, the surface coverage r of the measured region can be written as[43]

$$r = \frac{S_{\text{nano}}}{S_{\text{exciting}}}, \tag{2}$$

where S_{nano} and S_{exciting} represent the coverage area of the silver nanoflowers and the area of the whole image, respectively. For a quantitative comparison of the surface homogeneity of the two SERS substrates from different anodes, calculations were carried out based on the binarized SEM images, and the results are

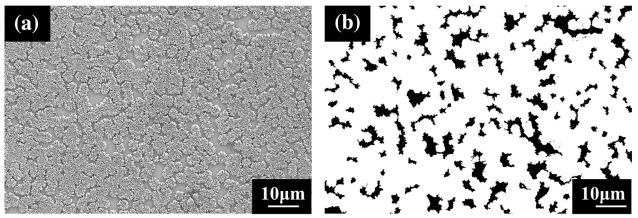

Fig. 8. SEM images used for surface coverage calculation: (a) gray-scale image; (b) binarized image.

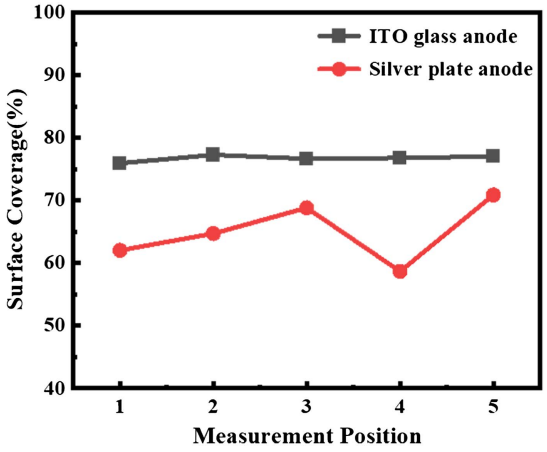

Fig. 9. Comparison of surface coverage of SERS substrates fabricated from the silver plate and ITO glass anodes.

shown in Fig. 9. As can be seen, the fluctuation of the surface coverage of the SERS substrate prepared with ITO glass is significantly smaller than that of the silver plate.

The SERS substrate surface homogeneity may be quantitatively evaluated as the following:

$$U = 1 - \frac{r_{\max} - r_{\min}}{r_{\text{av}}}, \tag{3}$$

where $r_{\max}$, $r_{\min}$, and r_{av} are the maximum, minimum, and average of the measured substrate surface coverages, respectively. Larger U value indicates better substrate uniformity. According to the data of Fig. 9, the surface homogeneity was calculated to be 81.2% and 98.3% for the SERS substrate from silver plate and ITO glass anodes, respectively. The dramatic difference in surface homogeneity spurred the motivation to explore the surface property of the anode plates.

4. Results and Discussion

4.1. Effect of the distance of electrodes on surface homogeneity

To study the effect of the distance of electrodes on surface homogeneity of the SERS substrate, the distance distribution between the two electrodes of the silver plate and the ITO glass needs to be analyzed. According to the measured results shown in Fig. 4, a simplified schematic representation of the distance of electrodes was established, as shown in Fig. 10. As the thickness of the spacer is 600 μm, $d = 600\,\mu\text{m}$ is selected as the reference distance, and then, the change of the distance is calculated. For the LC cell fabricated with silver plate, the minimum distance of electrodes should be $d - \Delta d_{\text{ITO}}$, and the maximum is $d + \Delta d_{\text{Ag}}$. Similarly, the distance between two ITO glass electrodes should lie in the interval $[d - 2\Delta d_{\text{ITO}}, d]$. With the established model, the deposited metal particles may be simulated according to Eq. (1), and then the surface homogeneity of the

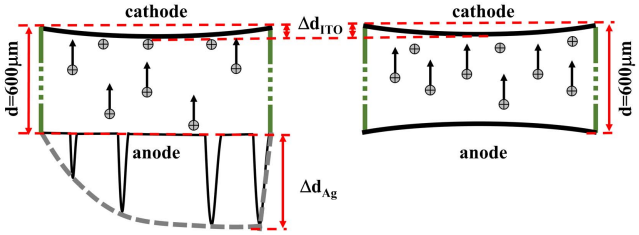

Fig. 10. Schematic diagram of the distance of electrodes with the silver plate (left) and the ITO glass (right) as the anode.

SERS substrate may be obtained. Moreover, by combining the measured distance variance (Fig. 4) and the surface coverage (Fig. 10), the effect of distance may also be evaluated to the surface coverage. To the silver plate, as the reference distance of 600 μm is the minimum distance of electrodes, the corresponding measured surface coverage should be maximum. But, the reference distance of 600 μm is the maximum distance of electrodes for the ITO glass anode, so it corresponds to the minimum measured surface coverage. Consequently, for the reference distance d equaling 600 μm, the reference surface coverages of the SERS substrates fabricated with silver plate and ITO glass are selected as the maximum and minimum values, respectively.

In order to evaluate the effect of distance on the surface homogeneity, the relative error φ was defined as

$$\varphi = \frac{|x - x_{\text{ref}}|}{x_{\text{ref}}}, \tag{4}$$

where x_{ref} is the variable at the reference position. First, according to the measured distance data, the relative error was computed based on the simulated deposition metal particles. Here, x is the number of deposited metal particles at different distances, and x_{ref} represents the number of metal particles deposited at the distance of 600 μm. The simulated results of the SERS substrates fabricated with the silver plate and ITO glass anodes are shown in Figs. 11(a) and 11(b), respectively. Further, the relative error of the surface coverage was also calculated, and here, x and x_{ref} are the measured and the reference surface

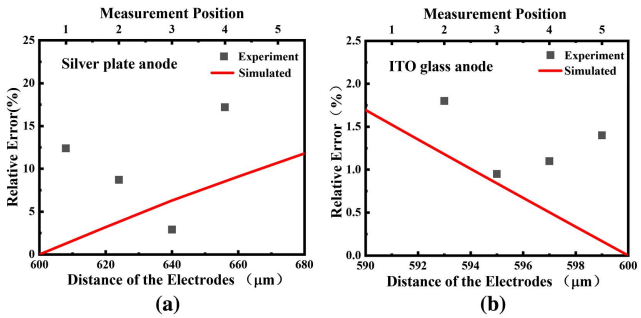

Fig. 11. Comparison of the simulation and experimental surface distribution uniformity of the SERS substrate fabricated from (a) a silver plate anode and (b) an ITO glass anode.

coverage of the SERS substrate, respectively. It is shown that, when the silver plate serves as the anode, the simulated relative error could reach 12%, while the experimental relative errors at the four other positions were 12.4%, 8.7%, 2.9%, and 17.2%, respectively. The larger experimental relative error might be caused by the complex surface morphology of the silver plate, which could bring about greater divergence in deposition speed. Similarly, when the ITO glass serves as the anode, only a tiny relative error of 1.7% could occur based on the simulated data, which accords with the experimental relative errors of 1.8%, 0.9%, 1.1%, and 1.4% at each position. In a word, the reasonably good match of the simulated and experimental relative errors about the surface distribution of the silver nanoparticles indicates the strong correlation between the electrode surface flatness and the deposited nanoparticle uniformity.

4.2. Raman spectrum uniformity of the SERS substrate

To investigate the effect of the electrode plate surface flatness on the SERS substrate Raman spectrum, Raman spectroscopy measurements were performed using a HORIBA LabRAM HR Raman spectrometer with the dye rhodamine 6G (R6G) as a probe. The working wavelength of Raman spectrometer is 532 nm. The integration time is 10 s. The laser power is 0.5 mW.

For a more convincing comparison, the positions measured in the Raman spectrometer measurements were the same as that of the SEM. Also, the Raman spectrum uniformity of the SERS substrates prepared using the silver plate or the ITO glass was compared. The coefficient of variation C_v is used to exhibit the spectrum uniformity of the SERS substrate, which is defined as[44]

$$C_v = \frac{\sigma}{\mu} \times 100\%, \tag{5}$$

where σ is the standard deviation of the Raman spectrum intensity. μ is the average of the Raman spectrum intensity.

As the substrates with deposited silver nanoparticles were designed for SERS, their enhancements in spectrum intensity were studied. The Raman spectra were collected at Positions 1–5 for both substrates under the same experimental conditions. With a R6G probe, sharp and strong Raman vibration peaks were detected at the SERS-active substrates [Figs. 12(a) and 12(b)]. The intensities of the strongest characteristic peaks at 613 cm^{-1} were checked and compared. To eliminate the single test error, a mean value for each position was concluded from five measurements at the same location. As shown in Fig. 12(c), the smaller spectrum intensity fluctuation was achieved when ITO glass served as the anode during electrodeposition. Concretely, benefitting from the more uniformly covered silver nanoflowers, a better spectrum uniformity was also realized for the ITO glass produced substrate, for which the coefficient of variation C_v was as small as 3.1%, while that associates with the silver plate significantly increased up to 14.9%. This reveals that the distance of electrodes could primarily affect the spectrum uniformity.

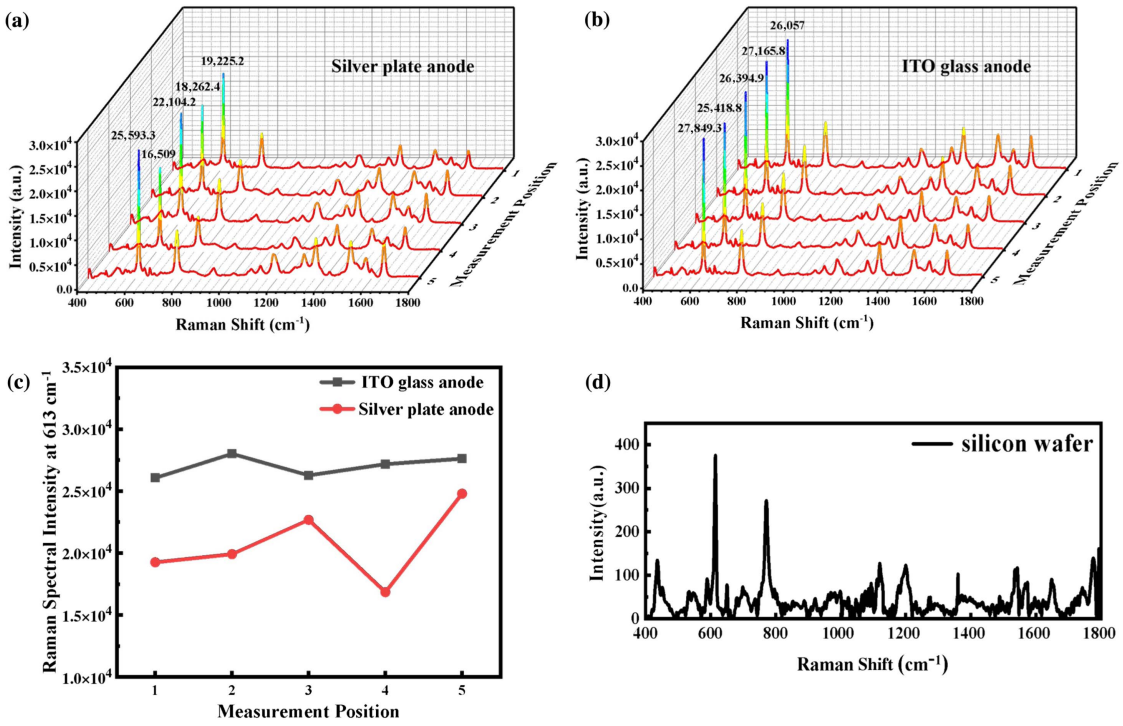

Fig. 12. Raman spectrum detected at different positions of the substrate fabricated from (a) a silver plate anode and (b) an ITO glass anode; (c) comparison of their peak intensities at 613 cm^{-1}; (d) Raman spectroscopy detection of R6G on a silicon wafer.

The enhancement effect of SERS material was evaluated by the enhancement factor (EF). R6G was used as the probe molecule in the experiment. Calculations were based on the following formula:

$$\mathrm{EF} = \frac{I_{\mathrm{SERS}}}{I_{\mathrm{bulk}}} \times \frac{Vc\delta N_A}{N_d A_N S}, \tag{6}$$

where I_{SERS} and I_{bulk} are the Raman spectral intensities measured by R6G on the SERS substrate and silicon wafer, respectively, V and c are the volume and concentration of R6G used on a silicon wafer, δ is the area occupied by the individual R6G molecules on the substrate, N_A is Avogadro's constant, N_d is the number density of the flower-like nanostructures on the substrate, A_N is the area of a single silver nanoflower, and S is the area of the R6G droplets on the substrate.

The EF for the SERS substrate was calculated from the Raman spectral intensity in Fig. 12. The average of the Raman spectral intensity on the surface of the SERS substrate was used as the value for I_{SERS}. Therefore, I_{SERS} of the silver plate as an anode is 20,338.8, and I_{SERS} of ITO glass as an anode is 26,577.2. The I_{bulk} value is 375.6. According to Eq. (6), the EF of the SERS substrate was 4.3×10^5 for the silver plate as the anode and 5.6×10^5 for the ITO glass as the anode.

5. Conclusions

In this study, we explored the effect of the surface flatness of the electrodes on the uniformity of metal particle distribution on the surface of the prepared SERS substrate, as well as the Raman spectrum intensity. Simulations were first performed to relate the electrode surface flatness to the number of deposited metal particles. To support the theoretical results, experiments were carried out with a rough and pitted silver plate anode or a smooth and slightly curved ITO glass anode during electrodeposition. According to SEM characterization and surface coverage calculation, higher surface homogeneity was achieved by the substrate fabricated from an ITO glass anode, which also showed a nice agreement with the simulations. More importantly, the SERS-active substrate obtained from flat ITO electrodes showed both high EF and excellent positional uniformity in the Raman spectrum. Our results not only evidenced the strong relationship between the electrode surface flatness and the SERS signal uniformity, but also opened an avenue for the fabrication of SERS-active substrates with high performance and low cost.

Acknowledgement

This work was supported by the Jiangsu Key Disciplines of the Fourteenth Five-Year Plan (No. 2021135), the National Natural Science Foundation of China (No. 22205155), the Natural Science Foundation of Jiangsu Province (No. BK20220640), and the Natural Science Foundation of Jiangsu Higher Education Institutions of China (No. 22KJB150011).

References

1. Y. Li, H. Chen, Y. Guo, K. Wang, Y. Zhang, P. Lan, J. Guo, W. Zhang, H. Zhong, and Z. Guo, "Lamellar hafnium ditelluride as an ultrasensitive surface-enhanced Raman scattering platform for label-free detection of uric acid," Photonics Res. **9**, 1039 (2021).
2. C. L. Huang, S. P. Jiang, F. X. Kou, M. T. Guo, S. Li, G. J. Yu, B. Zheng, F. Y. Xie, C. Zhang, H. L. Yu, and J. Wang, "Development of jellyfish-like ZnO@Ag substrate for sensitive SERS detection of melamine in milk," Appl. Surf. Sci. **600**, 154153 (2022).
3. L. Zhang, M. Q. Zhao, M. Xiao, M. H. Im, A. M. Abd El-Aty, H. Shao, and Y. X. She, "Recent advances in the recognition elements of sensors to detect pyrethroids in food: a review," Biosensors **12**, 402 (2022).
4. Y. Liu, Y. Chen, Y. Zhang, Q. Kou, Y. Zhang, Y. Wang, L. Chen, Y. Sun, H. Zhang, and Y. M. Jung, "Detection and identification of estrogen based on surface-enhanced resonance Raman scattering (SERRS)," Molecules **23**, 1330 (2018).
5. Z. Li, J. Wang, and D. Li, "Applications of Raman spectroscopy in detection of water quality," Appl. Spectrosc. Rev. **51**, 333 (2015).
6. S. E. J. Bell, G. Charron, E. Cortes, J. Kneipp, M. L. de la Chapelle, J. Langer, M. Prochazka, V. Tran, and S. Schlucker, "Towards reliable and quantitative surface-enhanced Raman scattering (SERS): from key parameters to good analytical practice," Angew. Chem. Int. Ed. **59**, 5454 (2020).
7. C. Cheng, J. Li, H. Lei, and B. Li, "Surface enhanced Raman scattering of gold nanoparticles aggregated by a gold-nanofilm-coated nanofiber," Photonics Res. **6**, 357 (2018).
8. A. Campion and P. Kambhampati, "Surface-enhanced Raman scattering," Chem. Soc. Rev. **27**, 241 (1998).
9. B. Sharma, R. R. Frontiera, A. I. Henry, E. Ringe, and R. P. Van Duyne, "SERS: materials, applications, and the future," Mater. Today **15**, 16 (2012).
10. H. Y. Chen, M. H. Lin, C. Y. Wang, Y. M. Chang, and S. Gwo, "Large-scale hot spot engineering for quantitative SERS at the single-molecule scale," J. Am. Chem. Soc. **137**, 13698 (2015).
11. C. Chen, Y. Li, S. Kerman, P. Neutens, K. Willems, S. Cornelissen, L. Lagae, T. Stakenborg, and P. Van Dorpe, "High spatial resolution nanoslit SERS for single-molecule nucleobase sensing," Nat. Commun. **9**, 1733 (2018).
12. H. K. Lee, Y. H. Lee, C. S. L. Koh, C. P. Q. Gia, X. M. Han, C. L. Lay, H. Y. F. Sim, Y. C. Kao, Q. An, and X. Y. Ling, "Designing surface-enhanced Raman scattering (SERS) platforms beyond hotspot engineering: emerging opportunities in analyte manipulations and hybrid materials," Chem. Soc. Rev. **48**, 731 (2019).
13. Y. N. Wang, M. Zhang, H. Ma, H. Y. Su, A. S. Li, W. D. Ruan, and B. Zhao, "Surface plasmon resonance from gallium-doped zinc oxide nanoparticles and their electromagnetic enhancement contribution to surface-enhanced Raman scattering," ACS Appl. Mater. Interfaces **13**, 35038 (2021).
14. L. M. Tong, T. Zhu, and Z. F. Liu, "Approaching the electromagnetic mechanism of surface-enhanced Raman scattering: from self-assembled arrays to individual gold nanoparticles," Chem. Soc. Rev. **40**, 1296 (2011).
15. C. H. Dai, Z. H. Lin, K. Agarwal, C. Mikhael, A. Aich, K. Gupta, and J. H. Cho, "Self-assembled 3D nanosplit rings for plasmon-enhanced optofluidic sensing," Nano Lett. **20**, 6697 (2020).
16. Y. T. Long, H. Li, Z. J. Du, M. M. Geng, and Z. R. Liu, "Confined Gaussian-distributed electromagnetic field of tin(II) chloride-sensitized surface-enhanced Raman scattering (SERS) optical fiber probe: from localized surface plasmon resonance (LSPR) to waveguide propagation," J. Colloid Interface Sci. **581**, 698 (2021).
17. S. Y. Ding, J. Yi, J. F. Li, B. Ren, D. Y. Wu, R. Panneerselvam, and Z. Q. Tian, "Nanostructure-based plasmon-enhanced Raman spectroscopy for surface analysis of materials," Nat. Rev. Mater. **1**, 16021 (2016).
18. A. Kaminska, I. Dziecielewski, J. L. Weyher, J. Waluk, S. Gawinkowski, V. Sashuk, M. Fialkowski, M. Sawicka, T. Suski, S. Porowski, and R. Holyst, "Highly reproducible, stable and multiply regenerated surface-enhanced Raman scattering substrate for biomedical applications," J. Mater. Chem. **21**, 8662 (2011).
19. V. T. N. Linh, J. Moon, C. Mun, V. Devaraj, J. W. Oh, S. G. Park, D. H. Kim, J. Choo, Y. I. Lee, and H. S. Jung, "A facile low-cost paper-based SERS substrate for label-free molecular detection," Sens. Actuators B **291**, 369 (2019).
20. X. Wang, L. Zhu, Z. Zhu, S. Chang, J. Qian, J. Jiang, X. Wang, A. Li, L. Jiang, and Y. Cao, "Simultaneously improved SERS sensitivity and thermal stability

on Ag dendrites via surface protection by atomic layer deposition," Appl. Surf. Sci. **611**, 155626 (2022).
21. S. R. Si, W. K. Liang, Y. H. Sun, J. Huang, W. L. Ma, Z. Q. Liang, Q. L. Bao, and L. Jiang, "Facile fabrication of high-density sub-1-nm gaps from Au nanoparticle monolayers as reproducible SERS substrates," Adv. Funct. Mater. **26**, 8137 (2016).
22. C. P. Zhang, S. Chen, Z. L. Jiang, Z. Y. Shi, J. L. Wang, and L. T. Du, "Highly sensitive and reproducible SERS substrates based on ordered micropyramid array and silver nanoparticles," ACS Appl. Mater. Interfaces **13**, 29222 (2021).
23. E. Murugan, S. Santhoshkumar, S. Govindaraju, and M. Palanichamy, "Silver nanoparticles decorated g-C_3N_4: an efficient SERS substrate for monitoring catalytic reduction and selective Hg^{2+} ions detection," Spectrochim. Acta Part A **246**, 119036 (2021).
24. X. F. Liu, J. M. Ma, P. F. Jiang, J. L. Shen, R. W. Wang, Y. Wang, and G. L. Tu, "Large-scale flexible surface-enhanced Raman scattering (SERS) sensors with high stability and signal homogeneity," ACS Appl. Mater. Interfaces **12**, 45332 (2020).
25. L. L. Zhang, X. D. Li, W. H. Liu, R. Hao, H. R. Jia, Y. Z. Dai, M. U. Amin, H. J. You, T. Li, and J. X. Fang, "Highly active Au NP microarray films for direct SERS detection," J. Mater. Chem. C **7**, 15259 (2019).
26. Y. Yu, P. Zeng, C. Yang, J. Y. Gong, R. Q. Liang, Q. R. Ou, and S. Y. Zhang, "Gold-nanorod-coated capillaries for the SERS-based detection of thiram," ACS Appl. Nano Mater. **2**, 598 (2019).
27. S. Lin, W. L. Hasi, X. Lin, S. Q. Han, T. Xiang, S. Liang, and L. Wang, "Lab-on-capillary platform for on-site quantitative SERS analysis of surface contaminants based on Au@4-MBA@Ag core-shell nanorods," ACS Sens. **5**, 1465 (2020).
28. G. Demirel, H. Usta, M. Yilmaz, M. Celik, H. A. Alidagi, and F. Buyukserin, "Surface-enhanced Raman spectroscopy (SERS): an adventure from plasmonic metals to organic semiconductors as SERS platforms," J. Mater. Chem. C **6**, 5314 (2018).
29. E. Cara, L. Mandrile, F. F. Lupi, A. M. Giovannozzi, M. Dialameh, C. Portesi, K. Sparnacci, N. De Leo, A. M. Rossi, and L. Boarino, "Influence of the long-range ordering of gold-coated Si nanowires on SERS," Sci. Rep. **8**, 11305 (2018).
30. C. Y. Gu, S. Q. Man, J. Q. Tang, Z. M. Zhao, Z. L. Liu, and Z. Y. Zheng, "Preparation of a monolayer array of silica@gold core-shell nanoparticles as a SERS substrate," Optik **221**, 165274 (2020).
31. V. Peksa, P. Lebruskova, H. Sipova, J. Stepanek, J. Bok, J. Homola, and M. Prochazka, "Testing gold nanostructures fabricated by hole-mask colloidal lithography as potential substrates for SERS sensors: sensitivity, signal variability, and the aspect of adsorbate deposition," Phys. Chem. Chem. Phys. **18**, 19613 (2016).
32. V. Suresh, L. Ding, A. B. Chew, and F. L. Yap, "Fabrication of large-area flexible SERS substrates by nanoimprint lithography," ACS Appl. Nano Mater. **1**, 886 (2018).
33. E. P. Kozhina, S. A. Bedin, N. L. Nechaeva, S. N. Podoynitsyn, V. P. Tarakanov, S. N. Andreev, Y. V. Grigoriev, and A. V. Naumov, "Ag-nanowire bundles with gap hot spots synthesized in track-etched membranes as effective SERS-substrates," Appl. Sci. **11**, 1375 (2021).
34. Z. X. Ye, L. Lin, Z. Y. Tan, Y. J. Zeng, S. C. Ruan, and J. Ye, "Sub-100 nm multi-shell bimetallic gap-enhanced Raman tags," Appl. Surf. Sci. **487**, 1058 (2019).
35. Y. Sanguansap, K. Karn-orachai, and R. Laocharoensuk, "Tailor-made porous striped gold-silver nanowires for surface enhanced Raman scattering based trace detection of beta-hydroxybutyric acid," Appl. Surf. Sci. **500**, 144049 (2020).
36. T. H. Wu and Y. W. Lin, "Surface-enhanced Raman scattering active gold nanoparticle/nanohole arrays fabricated through electron beam lithography," Appl. Surf. Sci. **435**, 1143 (2018).
37. G. J. Liu, K. G. Li, Y. B. Zhang, J. Du, S. Ghafoor, and Y. H. Lu, "A facile periodic porous Au nanoparticle array with high-density and built-in hot-spots for SERS analysis," Appl. Surf. Sci. **527**, 146807 (2020).
38. L. Zhang, W. Zhang, and F. Lu, "Azimuthal vector beam exciting silver triangular nanoprisms for increasing the performance of surface-enhanced Raman spectroscopy," Photonics Res. **7**, 1447 (2019).
39. L. Zhang, C. Meng, and G. Zhang, "Nanofocusing of a metallized double periodic arranged nanocone array for surface-enhanced Raman spectroscopy," Opt. Express **29**, 28086 (2021).
40. Y. Zhang, C. L. Yang, X. J. Xiang, P. G. Zhang, Z. H. Peng, Z. L. Cao, Q. Q. Mu, and L. Xuan, "Highly effective surface-enhanced fluorescence substrates with roughened 3D flowerlike silver nanostructures fabricated in liquid crystalline phase," Appl. Surf. Sci. **401**, 297 (2017).
41. Y. Zhang, C. L. Yang, B. Xue, Z. H. Peng, Z. L. Cao, Q. Q. Mu, and L. Xuan, "Highly effective and chemically stable surface enhanced Raman scattering substrates with flower-like 3D Ag-Au hetero-nanostructures," Sci. Rep. **8**, 898 (2018).
42. Q. Chen, C. Shi, L. Qin, S.-Z. Kang, and X. Li, "A low-cost 3D core-shell nanocomposite as ultrasensitive and stable surface enhanced Raman spectroscopy substrate," Sens. Actuators B **327**, 128907 (2021).
43. S. Zhang, Z. H. Jiang, Y. J. Liang, Y. L. Shen, H. M. Mao, H. J. Sun, X. Zhao, X. P. Li, W. S. Hu, G. D. Xu, and Z. L. Cao, "Effect of the duty cycle of flower-like silver nanostructures fabricated with a lyotropic liquid crystal on the SERS spectrum," Molecules **26**, 6522 (2021).
44. Z. H. Jiang, S. Zhang, H. M. Mao, H. J. Lu, X. P. Li, W. S. Hu, G. D. Xu, and Z. L. Cao, "Raman spectroscopic conformity of SERS substrate fabricated with lyotropic liquid crystal," Chin. J. Liq. Cryst. Disp. **37**, 806 (2022).